Prediction and Analysis of Durability Monitoring Data of High-Piled Wharf Based on GABP Neural Network Method

Hongbiao Liu, Zhixiang Wang, Huifang Liu*, Lei Zhang, Shuqing Ye and Pengrui Zhu

Abstract--**A durability monitoring system based on anode ladder sensors was deployed for the durability monitoring of high-piled wharf structures in Tianjin Port of China, and 4-years continuous monitoring data was collected. According to the analysis of monitoring data with the Pearson correlation coefficient, a strong correlation between the voltage and current values of anodes A1–A6 is proposed. Based on the monitoring data, the voltage and current values of anodes A1–A6 are predicted using the backpropagation (BP) neural network method, the particle swarm optimization-based BP method and the genetic algorithm-optimized BP method (GABP). The comparative analysis shows that the GABP method has the highest prediction accuracy, and the coefficient of determination (R^2) for the voltage and current predictions of anodes A1–A6 all exceed 0.80. This study provides a new approach for analyzing the durability monitoring data of coastal high-piled wharves.**

Index Terms—**anode ladder, high-piled wharf, neural network, Pearson correlation, durability monitoring**

I. Introduction

THE high-piled wharves of coastal port are crucial infrastructures for maritime transport and trade. The durability of concrete structures of wharves is a significant problem due to the long-term exposure to complex marine environments. Research indicates that the durability primarily depends on the concrete structural resistance to chloride ion penetration. Chloride ions gradually diffuse through the pores of the concrete surface to the surface of the reinforcement steel. Once chloride ions reach a certain concentration, the passive film on the steel surface will be destroyed, which causes the steel from a passive state to an active state, and resulting in depassivation or corrosion [1,2]. The process of steel from a passive state to an active state actually involves the formation of a macrocell corrosion system, where the active corroding areas (anodes) and the passive or slower corroding areas (cathodes) are connected electrically [3]. Measuring certain electrochemical parameters using sensors is often necessary to determine the specific corrosion conditions of steel reinforcement in concrete. Especially, one of the important methods for exploring steel corrosion in concrete is the corrosion current measurement.

Raupach and Schiessl [4] developed an anode ladder sensor system in 1986 and first applied it to actual engineering in 1990. This system was used to monitor the durability of concrete structures through macro-current systems, providing a new method for investigating reinforced concrete durability. By monitoring the transmission location of chloride ions with the anode-ladder system, Raupach and Schieβl [5] can determine the time when the reinforcement steel begins corrosion, and. the preventive measures can be taken before the concrete cracks and spalling. Chen et al. [6,7] used an embedded anode-ladder sensor to assess the corrosion risk of steel reinforcement in chloride environments based on the macro-current between the anode and cathode. Wang et al. and Li et al. [8,9] conducted monitoring research on the Sutong Bridge using the anode-ladder system, and corrected the functional relationship between corrosion mass loss after concrete cracking and macro-current by alternating wet–dry cycling tests. He et al. [10] evaluated the corrosion state of the reinforcement steel by monitoring data of the embedded anode-ladder system and using the half-cell potential method, and the relationship between electrochemical parameters and steel corrosion state was established. Based on the monitoring data, Liu et al. [11] found that the resistance of concrete is correlative with environmental temperature, and the current values of the anode-ladder sensor were influenced by temperature. Sun et al. [12] designed concrete test blocks based on actual engineering, and the anode-ladder system was deployed in the blocks. After several months of accelerated corrosion testing, the significant correlation between the potential of each anode rod and the depth of chloride ion penetration was found.

However, the durability monitoring of reinforcement concrete structures by the anode-ladder is a long-term process, and a large amount of monitoring data will be collected. Research indicates that the current values are often used to determine whether the anodes are in a de-passivated or corroded state. However, the current values can be influenced by related factors such as temperature and humidity, leading

Manuscript received November 16, 2024; revised June 4, 2025.

This study was funded by the National Key R&D Program of China (2022YFB3207400) and the Fundamental Research Funds for Central Public Research Institutes (TKS20230104).

Hongbiao Liu is a professor of Tianjin Research Institute for Water Transport Engineering, Tianjin 300456, China (e-mail: liuhbtks@163.com).

Zhixiang Wang is a postgraduate student of the Institute of Disaster Prevention, Sanhe 065201, Hebei, China (e-mail: wzxyyss@163.com).

Huifang Liu is a professor of Tianjin Research Institute for Water Transport Engineering, Tianjin 300456, China (corresponding author to provide phone: 86-15510867101; fax: 86-2259812373; e-mail: huifangliu2010@163.com).

Lei Zhang is an engineer of Unit 91053 of the Chinese People's Liberation Army, Beijing 100070, China (e-mail: pizi01213@163.com).

Shuqing Ye is a manager of the Zhoushan Yongzhou Container Terminal Co., Ltd., Zhoushan 316021, China (e-mail: 501628703@qq.com).

Pengrui Zhu is a professor of Tianjin Research Institute for Water Transport Engineering, Tianjin300456, China(e-mail:zprzprzpr@163.com).

to misjudgments when assessing the anode rod state [13-15]. Therefore, in order to reduce the misjudgment and make full use of monitoring data, this study employs Pearson correlation coefficients to analyze the correlation of the monitoring data collected from the anode-ladder and identify the main influence factors of the voltage and current values of the anode rods. Then, the nonlinear mapping and self-learning capabilities of neural networks were used to predict the voltage and current values of the anode ladder. A comparison of the prediction results of different models reveals that the GABP model has high predictive accuracy, and it has significant value in determining whether the anode rods are in de-passivated or corroded state.

II. Engineering Background

A. Anode Ladder Sensor Setup

A high-piled wharf is located in the Tianjin Port of China, which is used to handle bulk cargo. The wharf structure is designed for a 300,000 ton (DWT) bulk carrier. The total length and width of the wharf are 390m and 75m, respectively. The wharf comprises one main wharf platform and two lateral approach bridges, with the main platform measuring 390m in length and each approach bridge measuring 73.3 m. The main wharf platform is divided into nine structural segments, each 65m long, which is further subdivided into a front platform and a rear platform. The width of the front platform is 36.5 m, and the rear platform is slightly wider at 38.5m. In the front platform section, each structural segment is composed of 17 frames, with each frame containing 9 steel pipe piles, including 4 fork piles and 5 vertical piles. In the rear platform section, each frame consists of nine prestressed reinforced concrete square piles, each size 650 × 650 mm^2. The design load distribution of the wharf is segmented; starting from the front edge of the wharf, a uniform load of 30 kPa is applied within the first 18.5 m, followed by a load of 50 kPa for the next 18 m (from 18.5 m to 36.5 m), and a load of 80 kPa from 36.5 m to the end of the wharf (75 m). Additionally, the wharf is equipped with a structural health monitoring system installed on the second structural segment. The specific layout of the durability sensors on the wharf is illustrated in Fig.1.

B. Sensor-related information

During its initial establishment, the German-manufactured anode ladder sensor (produced by Sensortec GmbH in 2016) was employed in the wharf for monitoring structural durability. This system consisted of several key components: the anode ladder embedded in the concrete, external testing interfaces, and specialized data acquisition equipment. The anode ladder sensor comprised multiple components, including anode rods, a cathode, a reference electrode, a steel rod for reinforcement connection(CR), and a temperature probe (PT1000). The anode ladder consisted of six anodes made of carbon steel, labeled A1–A6. These anode rods were embedded at varying depths within the concrete cover by adjusting the tilt angle of the brackets. The specific installation method and side view are displayed in Fig. 2. The basic monitoring principle was as follows: The onset of corrosion for each could be monitored by arranging electrodes at different depths on the concrete surface. The extent of chloride ion diffusion in the concrete could be accurately determined by measuring key parameters such as the potential, current, resistance, and temperature of the anodes at varying depths. The initiation time of steel corrosion could be further predicted based on the monitoring data [16-18].

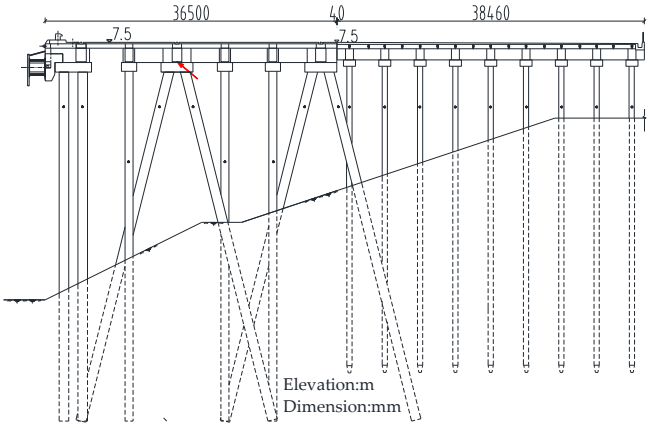

Fig. 1. Cross section of the South 27# Wharf

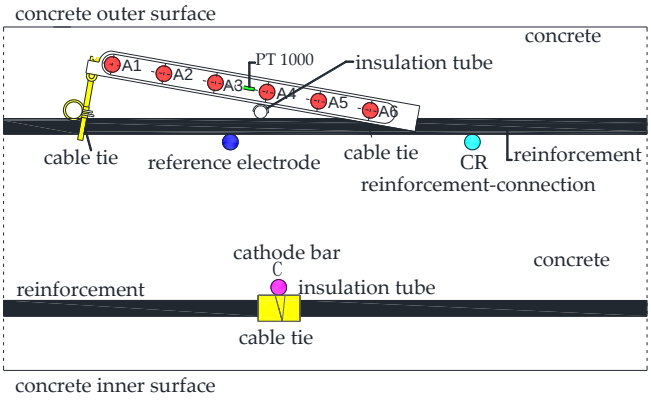

(a) Side view of anode ladder

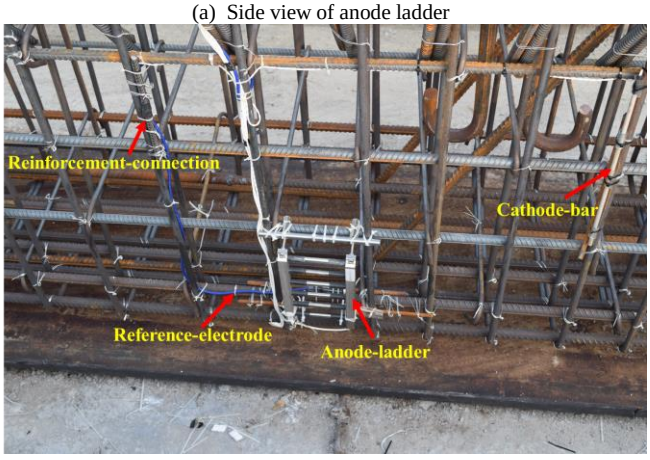

(b) Installation of anode ladder

Fig. 2. Anode ladder sensor

C. Long-term monitoring data

After the completion of the main structure of the wharf at Tianjin Port, data col-lection using the anode ladder sensors was commenced. The construction of this wharf project began in early 2016 and was completed by 2017. Subsequently, data collection from the anode ladder sensors officially started in January 2018 and continued for 4 years, during which data on 40 different parameters were collected. The recorded parameters were as follows: the voltage values of the anode

rods relative to the cathode, reference electrode, and internal steel reinforcement, as well as current values relative to the cathode and internal steel reinforcement, along with environmental temperature values, as illustrated in Fig.3. This study focused on the predictive analysis of the voltage and current values for anodes A1–A6. Specific data are detailed in Table I and Fig.4. The durability monitoring data collected were standardized and stored in the health monitoring system and operation platform, enabling automated display and analysis, thus providing strong data support for the operation and maintenance management of wharf.

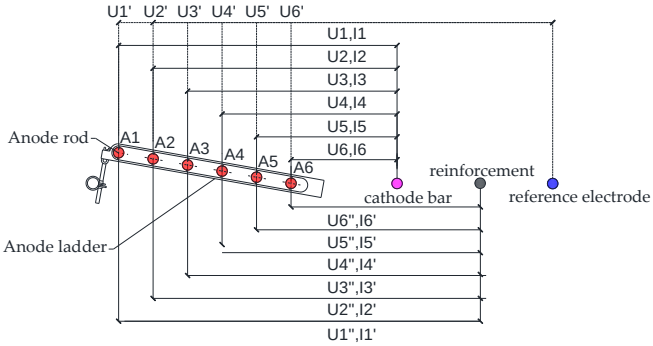

Fig. 3. Anode rods A1–A6 monitoring parameter description diagram

D. Evaluation methods

The laboratory test results indicated that when the anode was short-circuited with the cathode in dry concrete for 5s, a voltage of 150mV or a current of 15 μA between the anode and the cathode could be considered as the threshold for the anode to be in an active state. However, these thresholds may be higher in humid environments, such as marine conditions[5,15]. This finding aided in determining the active state of the anode and predicting the critical depth at which steel corrosion might occur.

The ASTM C876-09 standard [19] provides another method for assessing the corrosion state of reinforcement steel, known as the half-cell potential method. This method measures the half-cell potential of the steel reinforcement related to the concrete surface using a copper–copper sulfate half-cell on the wet concrete surface. According to the standard, if the half-cell potential is below –0.35V, the corrosion probability of reinforcing steel is more than 90%. If the half-cell potential is positive or falls between –0.35V and –0.2V, the results cannot definitively determine the corrosion state of the steel. When the half-cell potential is between –0.2 V and 0 V, the probability of steel corrosion is less than 10%, as detailed in Table Ⅱ.

TABLE Ⅱ
CORROSION PROBABILITY OF REINFORCING STEEL

Half-cell potential (V)	More negative than 0.35 V	–0.35 V to –0.2 V	More positive than –0.20 V
Corrosion probability of steel in one area	> 90%	Uncertain	< 10%

TABLE I
VOLTAGE AND CURRENT VALUES COLLECTED USING THE ANODE LADDER SENSOR

	No.	Name	Description	No.	Name	Description	No.	Name	Description
U/mV	1	U1	Voltage between A1 and cathode	7	U1′	Voltage between A1 and reference electrode	13	U1′′	Voltage between A1 and reinforcement connection
	2	U2	Voltage between A2 and cathode	8	U2′	Voltage between A2 and reference electrode	14	U2′′	Voltage between A2 and reinforcement connection
	3	U3	Voltage between A3 and cathode	9	U3′	Voltage between A3 and reference electrode	15	U3′′	Voltage between A3 and reinforcement connection
	4	U4	Voltage between A4 and cathode	10	U4′	Voltage between A4 and reference electrode	16	U4′′	Voltage between A4 and reinforcement connection
	5	U5	Voltage between A5 and cathode	11	U5′	Voltage between A5 and reference electrode	17	U5′′	Voltage between A5 and reinforcement connection
	6	U6	Voltage between A6 and cathode	12	U6′	Voltage between A6 and reference electrode	18	U6′′	Voltage between A6 and reinforcement connection
I/μA	1	I1	Current between A1 and cathode	7	I1′	Voltage between A1 and reinforcement connection			
	2	I2	Current between A2 and cathode	8	I2′	Voltage between A2 and reinforcement connection			
	3	I3	Current between A3 and cathode	9	I3′	Voltage between A3 and reinforcement connection			
	4	I4	Current between A4 and cathode	10	I4′	Voltage between A4 and reinforcement connection			
	5	I5	Current between A5 and cathode	11	I5′	Voltage between A5 and reinforcement connection			
	6	I6	Current between A6 and cathode	12	I6′	Voltage between A6 and reinforcement connection			
T/C°	Concrete temperature value (PT1000)								

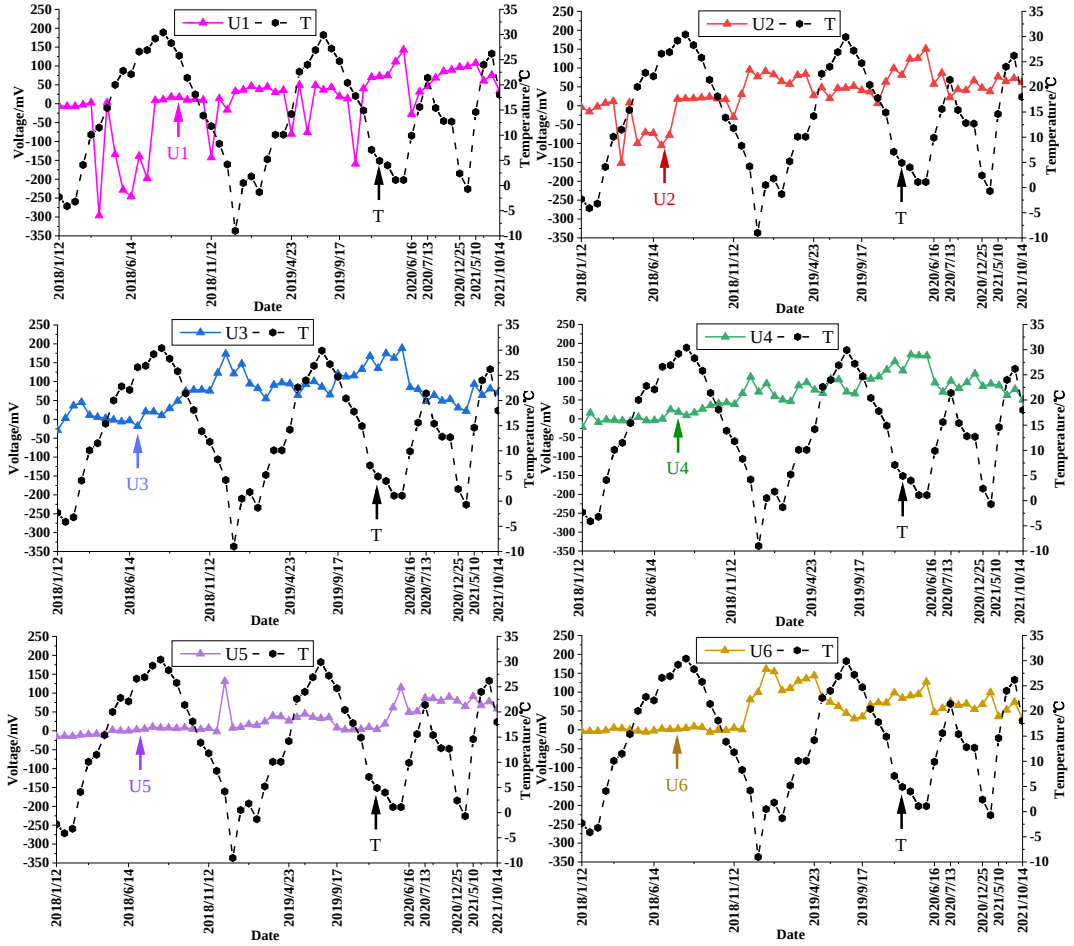

(a) Voltage between anode and cathode

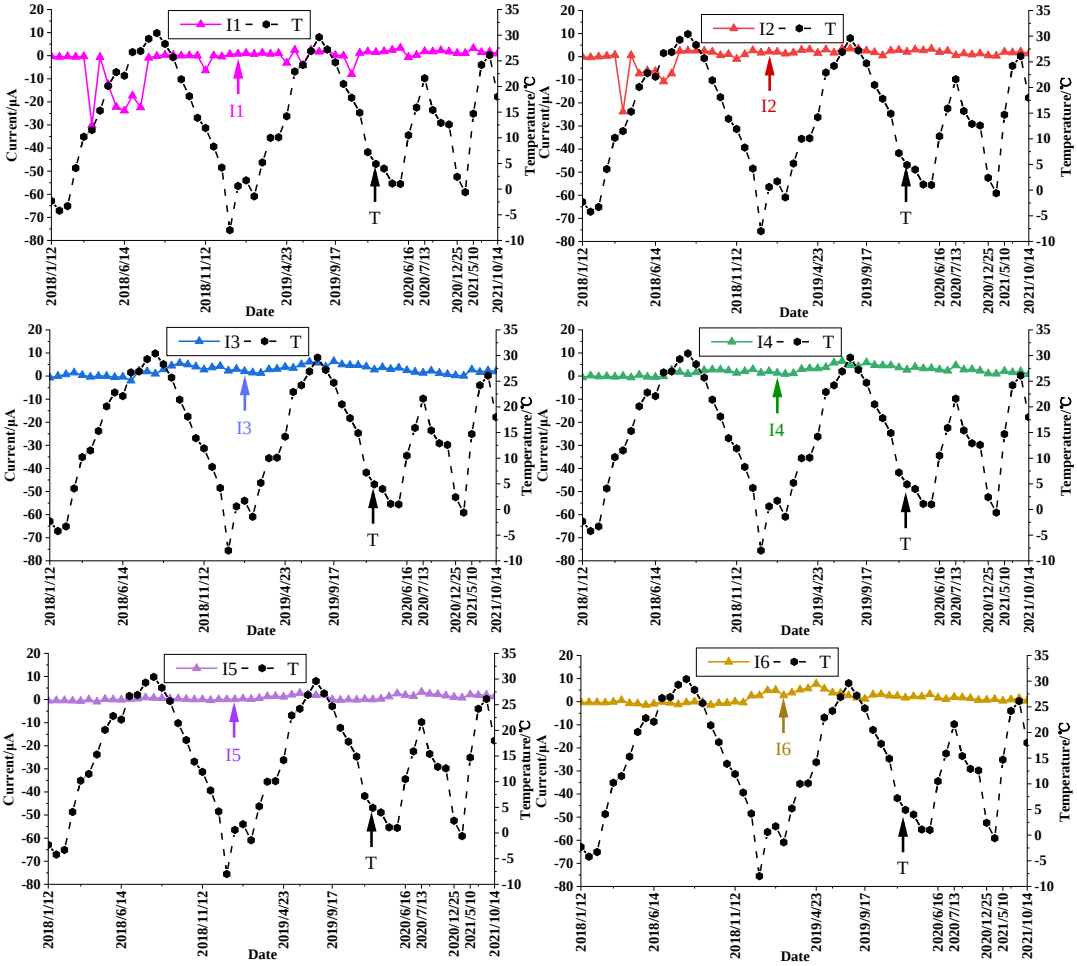

(b) Current between anode and cathode

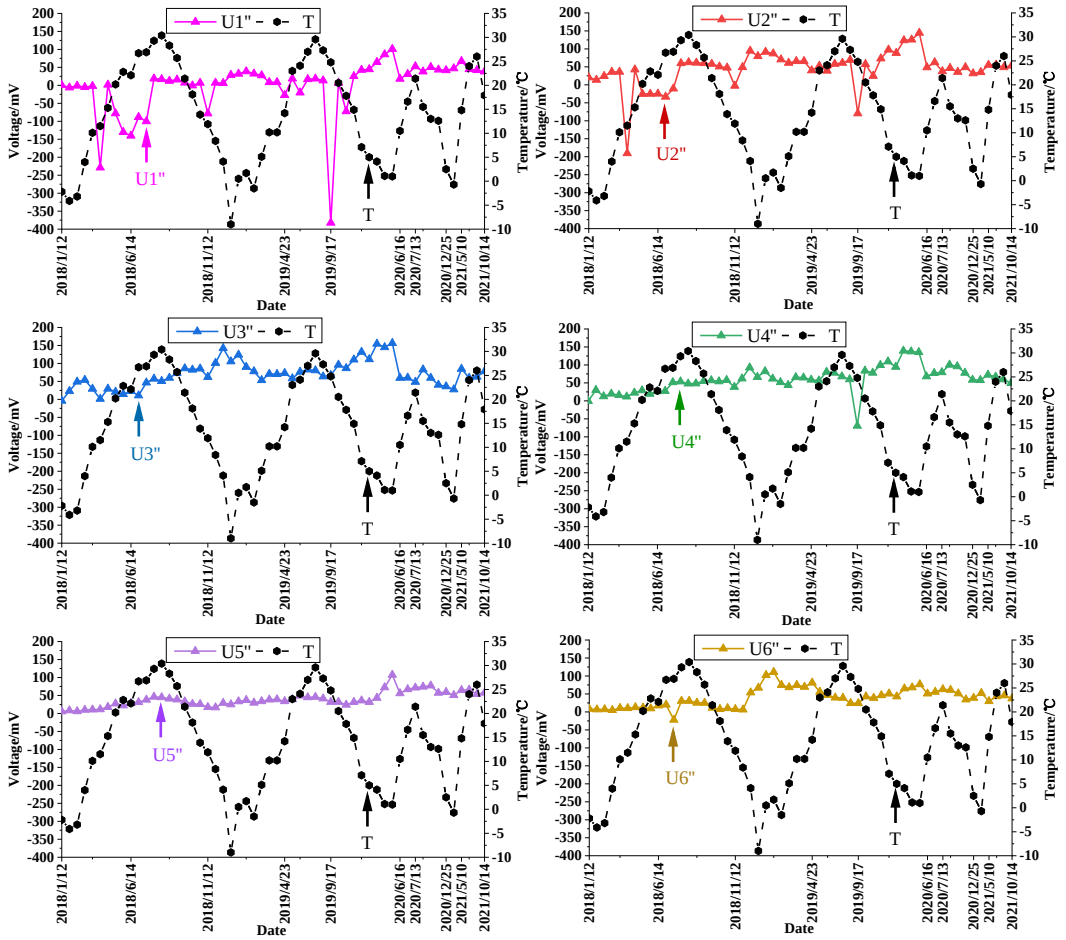

(c) Voltage between the anode and reinforcement-connection

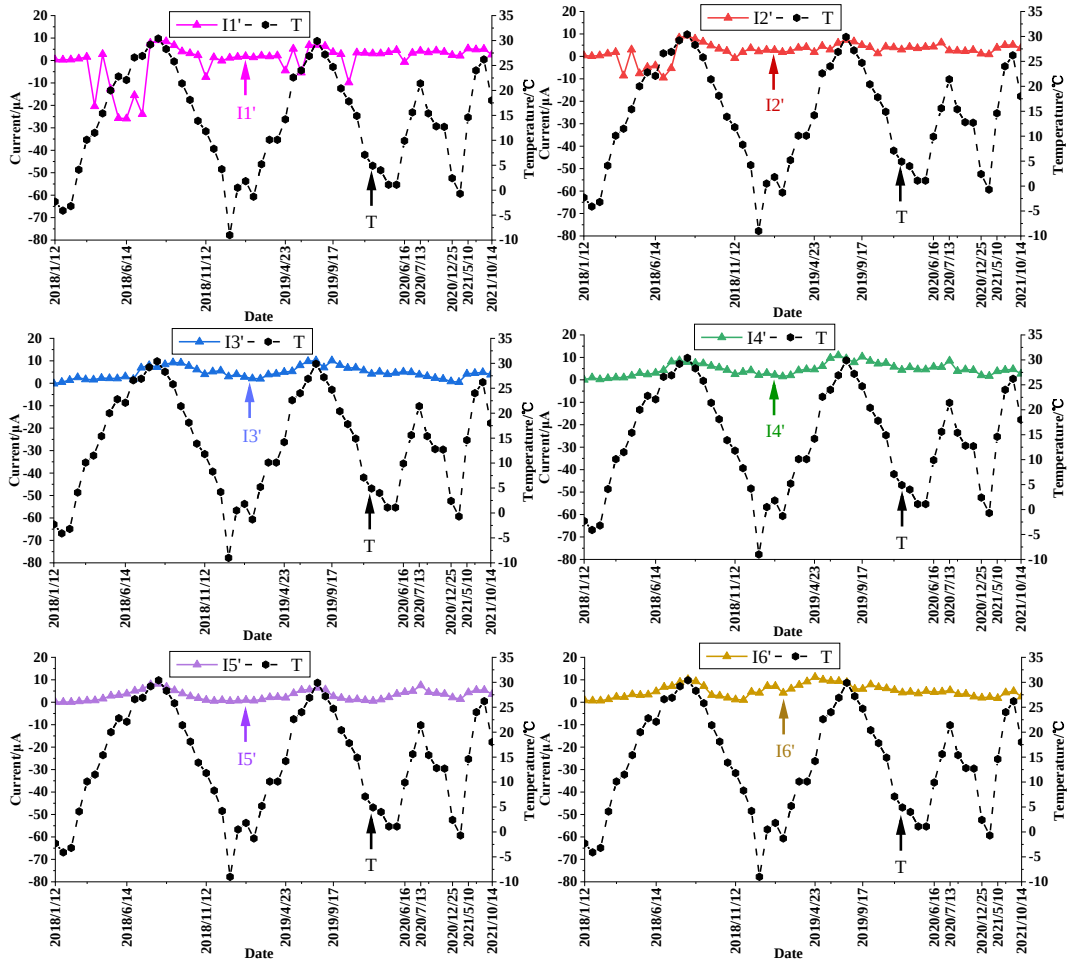

(d) Current between the anode and reinforcement-connection

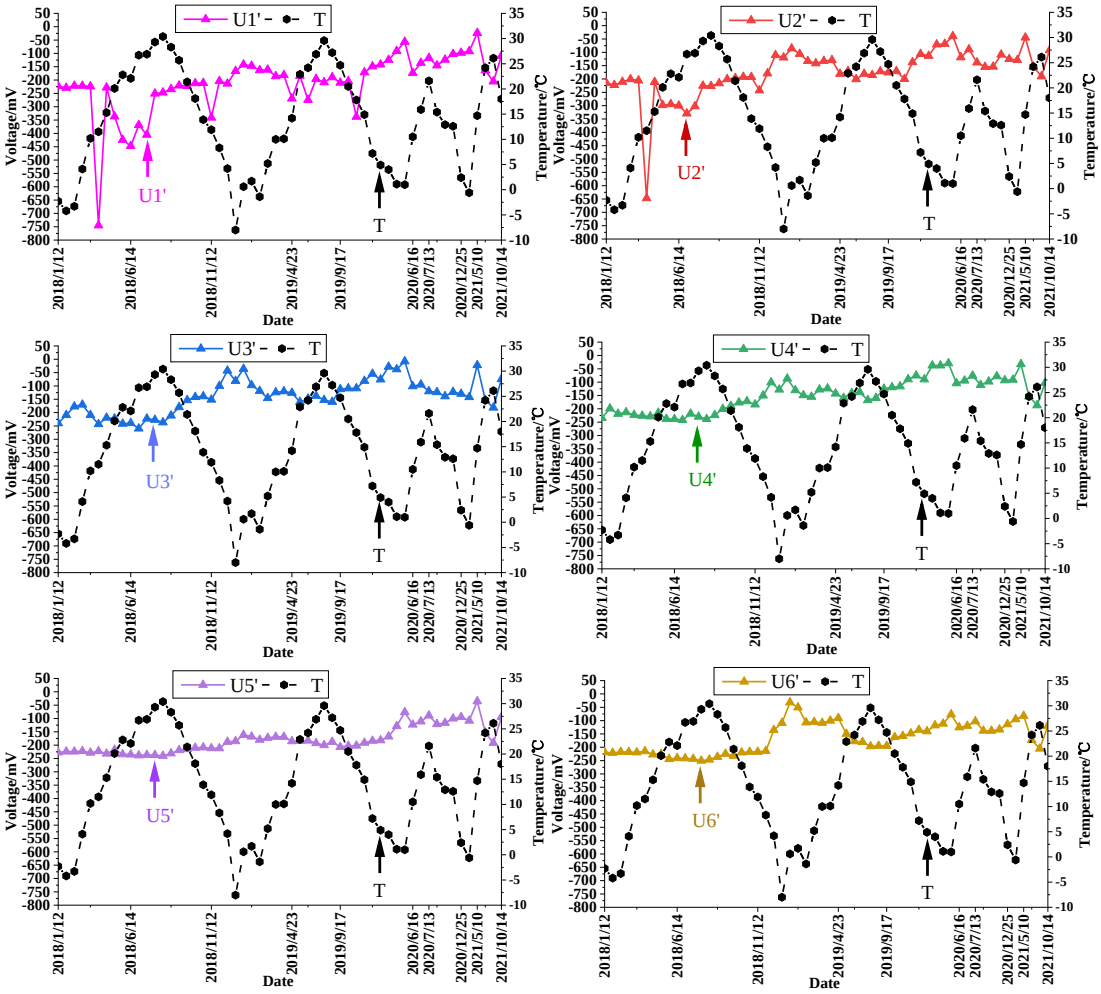

(e) Voltage between the anode and reference-electrode

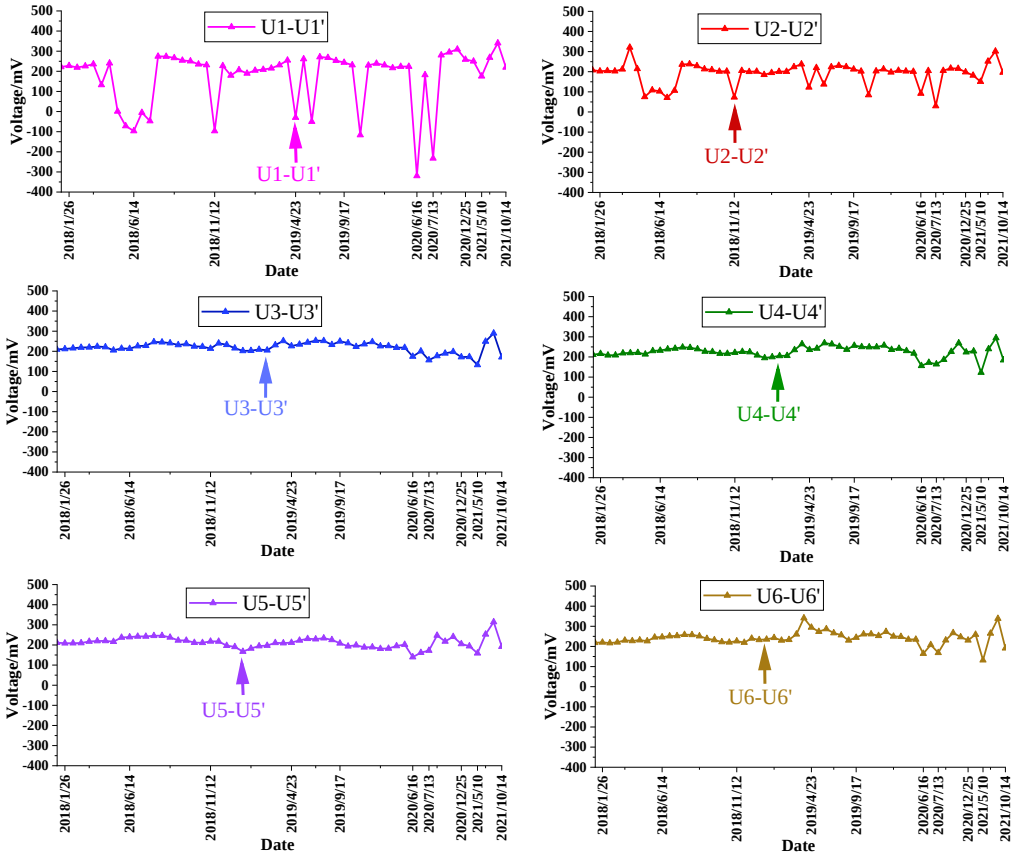

(f) Potential difference between the anode and reference-electrode

Fig. 4. Anode ladder collecting raw data

III. Prediction Methodology

The prediction method of anode ladder voltage and current value based on the GABP neural network mainly included the following three parts:

(1) Pearson correlation coefficient was used to calculate the original data and determine the correlation between various factors.

(2) While constructing the GABP neural network model, a genetic algorithm was used to optimize the global search ability, and the optimal weights and thresholds were obtained through continuous iterative optimization. This improved the generalization performance and learning speed of the model.

(3) Regardless of the voltage and current values of the anode rods A1–A6 relative to the cathode or the voltage and current values relative to the steel bar were positively correlated, which conformed to the correlation law of voltage and current in physics and also verified the reliability of the monitoring data of the anode-ladder sensor.

A. Correlation analysis of monitoring data

Specific values for voltages U1–U6, currents I1–I6, voltages U1′–U6′, voltages U1′′–U6′′, currents I1′–I6′, and ambient temperature T could be obtained over a continuous period of 4 years based on the monitoring data shown in Table I for the anode ladder. The correlations between these factors were analyzed using the Pearson correlation coefficient [shown in Eq. (1)] to identify the main factors influencing the variations in anode rod voltage and current values.

$$r=\frac{\sum_{i=1}^{n}(x_i-\bar{x})(y_i-\bar{y})}{\sqrt{\sum_{i=1}^{n}(x_i-\bar{x})^2(y_i-\bar{y})^2}} \quad (1)$$

where r represents the correlation coefficient, x_i and y_i denote the actual values of the respective factors, $\bar{x}$ and $\bar{x}$ represent the mean values of these factors, and n indicates the number of data points. Fig.5 illustrates the correlation coefficients between anode voltage and current values and other factors. The value of r ranges from 0 to 1; if $r > 0$, a positive correlation exists between the two variables, whereas if $r < 0$, a negative correlation exists. The greater the absolute value of r, the stronger the correlation. If $r = 0$, no linear correlation exists between the two. Generally, a correlation coefficient of 0.0~0.2 indicates no correlation or very weak correlation, 0.2~0.4 indicates weak correlation, 0.4~0.6 indicates moderate correlation, 0.6~0.8 indicates strong correlation, and 0.8~1.0 indicates very strong correlation [20-22].

The results of monitoring data calculated using the Pearson correlation coefficient are shown in Fig.5, leading to the following conclusions:

(1) The calculated correlation coefficients between the anode voltage values U1–U6 and current values I1–I6 were all more than 0.85, indicating a very strong correlation between the variables.

(2) The graph in Fig.5f shows that despite no significant potential difference between the anode rods A1–A6 and the cathode or reference electrode, the correlation coefficients between the anode voltage values U1–U6 and the reference electrode voltage values U1′–U6′ were all more than 0.7, indicating a strong correlation.

(3) Both the voltage and current values of the anode rods A1–A6 relative to the cathode and the voltage and current values relative to the reinforcing bars were positively correlated, consistent with the physical relationship between voltage and current. This also verified the reliability of the monitoring data from the anode ladder sensors.

B. Backpropagation neural network

The monitoring dataset used in this study for the anode ladder exhibited nonlinear characteristics, and the BP neural network demonstrated excellent performance in predicting such datasets, having matured significantly in the field of machine learning. Therefore, this study selected the BP neural network method to predict the voltage and current values of the anode ladder [23].

The backpropagation (BP) neural network consisted of an input layer, hidden layers, and an output layer, with each layer containing multiple neurons. The number of these neurons was determined based on empirical formulas. This network model possessed the ability to approximate any function, allowing it to learn nonlinear relation-ships and exhibit a certain level of generalization capability. During its training process, the BP algorithm was employed to continually adjust the weights w and thresh-olds θ within the network to minimize the loss function, thereby ensuring that the network's output closely approximated the true values. The algorithmic process is de-tailed as follows [24-26].

1) Normalization of raw data

Before conducting calculations, the raw data must be normalized to facilitate sub-sequent data processing and increase the convergence speed of the program. The formula for data normalization is given by:

$$X'=(Y_{max}-Y_{min})\frac{X_i-X_{min}}{X_{max}-X_{min}}+Y_{min} \quad (2)$$

where Y_{max} and Y_{min} are defined as fixed upper and lower bounds, respectively, which were chosen in this study to be [0, 1]; X_{max} and X_{min} represent the maximum and minimum values from original data, respectively, and $X_{min} \leqslant X' \leqslant X_{max}$.

2) Activation function selection and parameter tuning

Common activation functions used in artificial neural networks include Sigmoid, Tanh, and ReLU. After preliminary calculations, this study ultimately selected the Sigmoid function as the activation function. The selection of the number of neurons is a complex issue; this study employed the empirical formula (3) to determine the number of neurons.

$$N=\sqrt{n+m}+a \quad (3)$$

where n represents the number of input units, m denotes the number of output neurons, and a is a constant between [1, 10]. In this study, the number of input units was 5, the number of output neurons was 1, and a was set to 5. The flowchart of the BP neural network is illustrated in Fig.6.

C. GABP neural network

However, the BP neural networks use the gradient descent

method to adjust weights and thresholds and hence are prone to getting stuck in local optima. GABP is an improved neural network model that combines the advantages of genetic algorithms and BP neural networks. In the GABP model, the genetic algorithm is used to optimize global search capability, thereby avoiding the issue of the BP neural network falling into local optima, subsequently enhancing the model's stability. The model's generalization ability and learning speed could be improved by updating weights and thresholds, especially when dealing with complex nonlinear problems and large-scale datasets, showing significant advantages [27].

When optimizing BP neural networks with genetic algorithms, specific parameter values, such as the size of the initial population, the maximum number of evolution generations, the crossover rate, and the mutation rate, should be determined. The de-termination of these parameters relies on the designer's experience and multiple trials. In this study, the set values were 30, 50, 0.8, and 0.2, respectively. The flowchart of the GABP neural network is shown in Fig.7 [28,29].

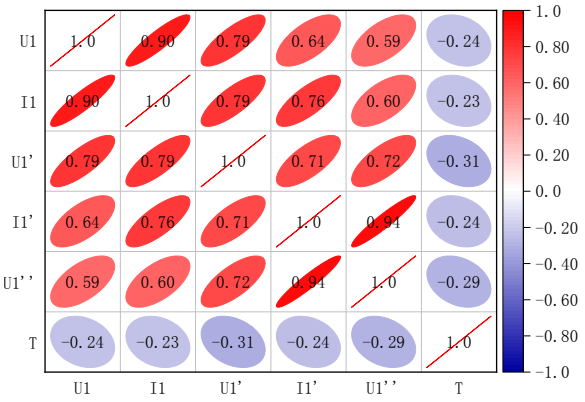

(a) Anode rod A1 data correlation

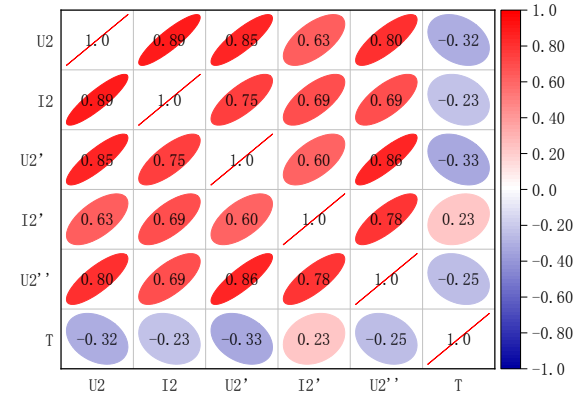

(b) Anode rod A2 data correlation

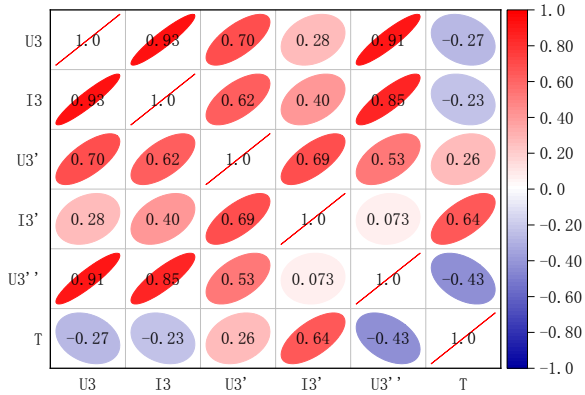

(c) Anode rod A3 data correlation

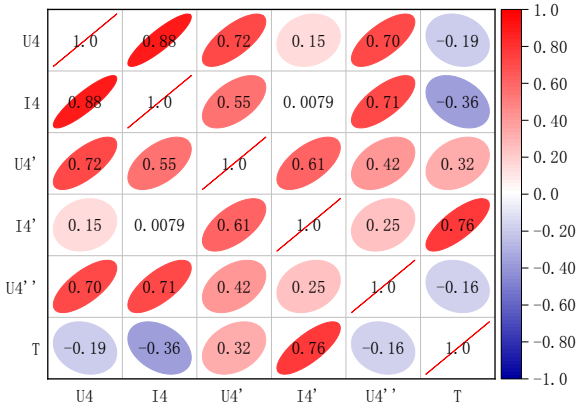

(d) Anode rod A4 data correlation

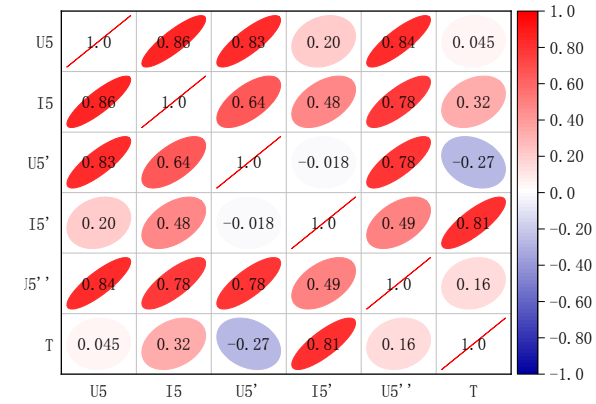

(e) Anode rod A5 data correlation

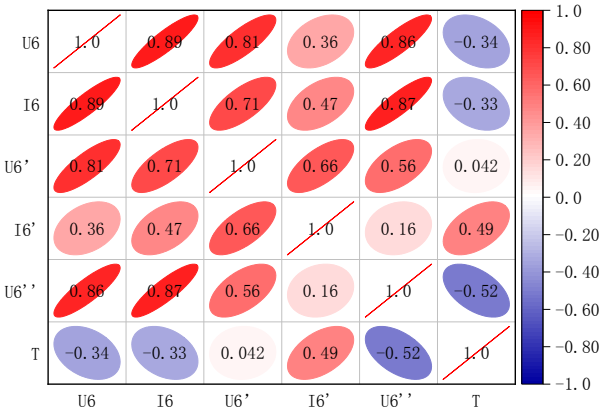

(f) Anode rod A6 data correlation

Fig. 5. Pearson correlation analysis of data

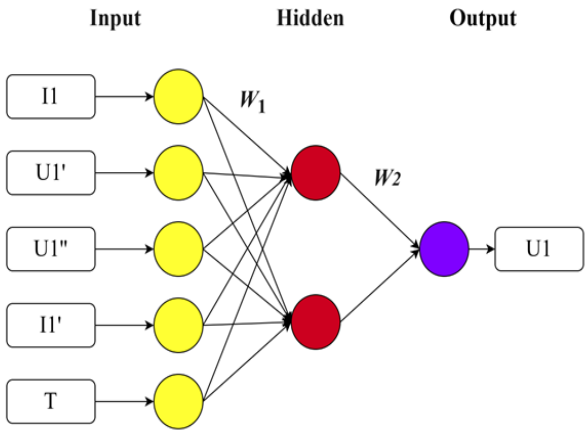

Fig. 6. BP neural network structure

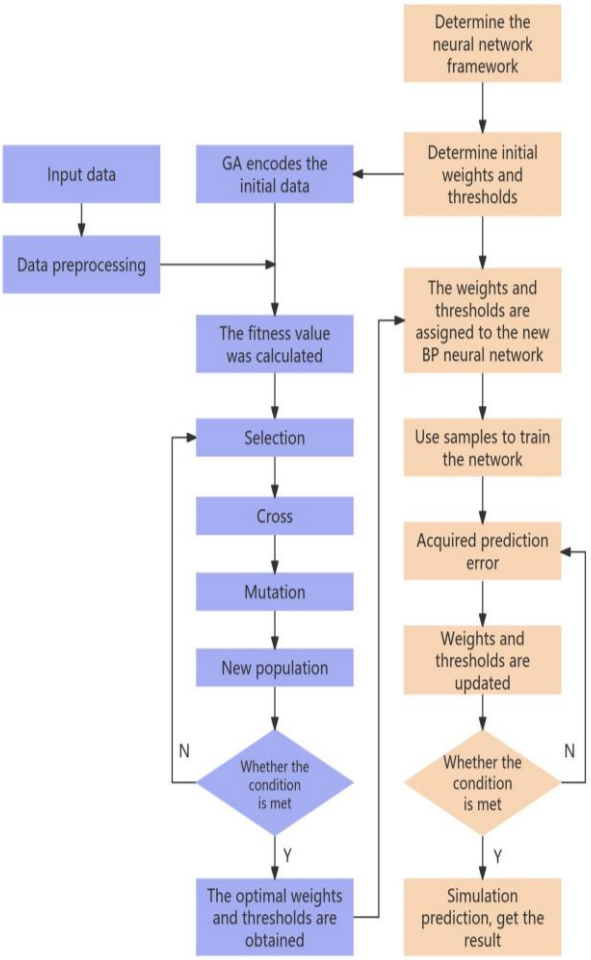

Fig. 7. GABP neural network structure

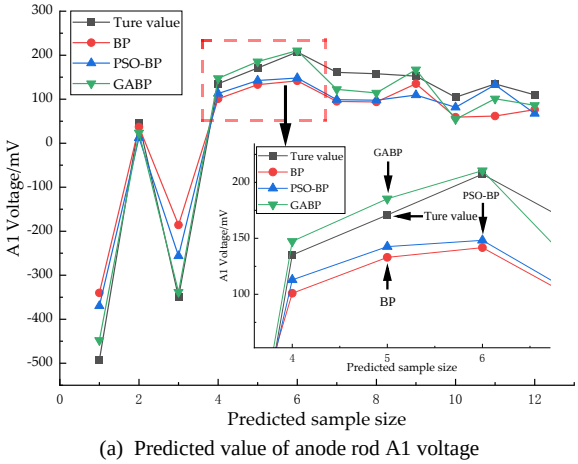

(a) Predicted value of anode rod A1 voltage

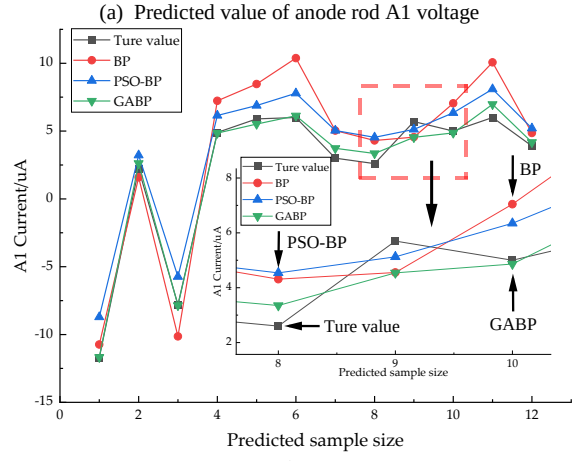

(b) Predicted value of anode rod A1 current

Fig. 8. Predicted voltage and current value

IV. Results and Analysis

A. Voltage and current value prediction verification

The voltage and current values of the anode rods were predicted based on the conclusions drawn from the aforementioned analysis and the established model. When predicting the voltage value U1 of anode rod A1, the current value I1, voltage value U1′, voltage value U1′′, current value I1′, and ambient temperature T were used as input variables. From the 56 samples of the original data, 80% were selected as the training set and the remaining 20% as the testing set [30,31]. The other five related factors were similarly selected as input variables for predicting the current value I1 of anode rod A1. Predictions were conducted using the BP neural network, particle swarm optimization BP neural network, and genetic algorithm–optimized BP neural network models to better assess the model's effectiveness and optimization results. A comparative analysis of the predicted results was performed. The predicted voltage and current values for anode rod A1 are presented in Table Ⅲ and Fig.8.

Based on the aforementioned prediction results, the error analysis of the model was conducted using the calculated results of the root mean square error (RMSE), mean absolute error (MAE), coefficient of determination (R^2), and mean square relative error (MSRE). RMSE and MAE are commonly used to measure the difference be-tween predicted values and actual measurements. R^2 assesses the goodness of fit of the model, with results closer to 1 indicating a better fit. MSRE reflects the model's performance in predicting relative errors. The calculation formulas are shown in Eqs. (4) to (7):

$$RMSE=\sqrt{\frac{1}{n}\sum_{i=1}^{n}(y_i-\hat{y}_i)^2} \tag{4}$$

$$MAE=\frac{1}{n}\sum_{i=1}^{n}\left|y_i-\hat{y}_i\right| \tag{5}$$

$$R^2=1-\frac{\sum_{i=1}^{n}(y_i-\hat{y}_i)^2}{\sum_{i=1}^{n}(y_i-\bar{y}_i)^2} \tag{6}$$

$$MSRE=\frac{1}{n}\sqrt{\sum_{i=1}^{n}\left[\frac{(y_i-\hat{y}_i)}{y_i}\right]^2} \tag{7}$$

where y_i represents the actual recorded values of voltage and current for the i measurement of the anode rod A1, $\hat{y}_i$ denotes the predicted values for the i voltage and current, $\bar{y}_i$ indicates the average actual recorded values of all test samples, and n is the total number of predicted values for voltage and current.

Equations (4)~(7) were used for error calculation and analysis. The prediction results of the three methods are presented in Table Ⅳ. The comparison of error values is shown in Fig.9. Table Ⅳ shows that the R^2 for predicted voltage values of the GABP model was 14% higher than that of the BP neural network model and 5% higher than that of the PSO-BP neural network model. For the current values, the R2 of the GABP model was 21% higher than that of the BP neural

TABLE Ⅲ
SUMMARY OF MODEL PREDICTIONS

No.	Anode rod A1 true value		BP predicted value		PSO-BP predicted value		GABP predicted value	
	Voltage value	Current value	Voltage value	Current value	Voltage value	Current value	Voltage value	Current value
1	–493.00	–11.7	–340.13	–10.74	–369.83	–8.71	–447.81	–11.67
2	46.40	2.2	37.01	1.59	12.34	3.22	23.69	2.62
3	–349.30	–7.8	–185.78	–10.14	–256.22	–5.73	–338.25	–7.85
4	135.20	4.9	100.96	7.23	112.90	6.15	147.32	4.85
5	170.90	5.9	133.00	8.47	142.56	6.89	185.33	5.52
6	207.30	6	141.69	10.38	148.24	7.79	210.49	6.13
7	161.10	3	95.02	5.04	98.93	5.04	122.23	3.73
8	157.80	2.6	93.72	4.31	97.69	4.54	114.38	3.35
9	152.30	5.7	135.22	4.55	109.43	5.13	167.12	4.54
10	104.50	5	59.28	7.04	81.47	6.35	54.38	4.86
11	134.70	6	61.83	10.06	132.58	8.09	101.15	6.97
12	109.90	3.9	76.31	4.86	67.40	5.21	86.05	4.17

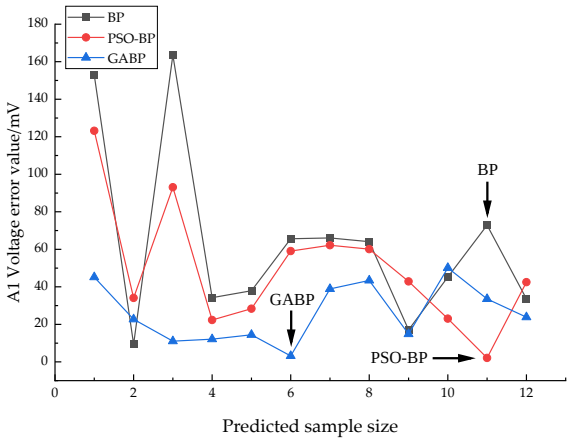

(a) Anode rod A1 voltage prediction error value

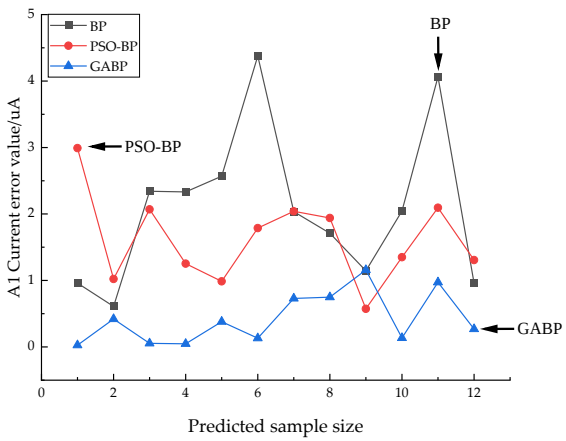

(b) Anode rod A1 current prediction error value

Fig. 9. Error of the predicted values of the three models

TABLE Ⅳ
SUMMARY OF ERRORS IN MODEL PREDICTIONS

Model	RMSE		MAE		R^2		MSRE	
	Voltage value	Current value	Voltage value	Current value	Voltage value	Current value	Voltage value	Current value
BP	78.72	2.38	63.54	2.10	0.86	0.81	1.76	1.11
PSO-BP	58.77	1.74	49.40	1.62	0.92	0.90	1.31	0.81
GABP	30.10	0.56	26.11	0.42	0.97	0.98	0.67	0.26

TABLE Ⅴ
A2-A6 ERROR CALCULATION SUMMARY TABLE

No.	RMSE		MAE		R^2		MSRE	
	Voltage value	Current value	Voltage value	Current value	Voltage value	Current value	Voltage value	Current value
A2	20.65	0.46	17.35	0.40	0.90	0.92	0.33	0.16
A3	11.95	0.53	10.34	0.45	0.82	0.90	0.16	0.20
A4	13.59	0.34	11.15	0.22	0.86	0.94	0.13	0.10
A5	13.25	0.35	10.38	0.31	0.84	0.92	0.14	0.11
A6	12.35	0.34	10.47	0.29	0.88	0.85	0.13	0.12

network model and 9% higher than that of the PSO-BP neural network model. Therefore, the prediction performance of the GABP method significantly outperformed the performance of other methods, further validating the feasibility and effectiveness of the prediction approach.

B. Model generalization verification

The prediction method was applied to the monitoring data of the anode rod A1 to predict the actual voltage and current values of anode rods A2–A6 so as to verify the generalization performance of the GABP model. Subsequently, error analysis was conducted using RMSE, MAE, R^2, and MSRE. The specific results are presented in Table Ⅴ.

The error analysis of the voltage and current prediction results for anode rods A2–A6 in Table Ⅴ shows that the R^2 values were all more than 0.80. This indicated that the GABP model possessed high prediction accuracy and also reflected the model's practicality and generalization performance.

V. CONCLUSION

Currently, there are few related research on the durability of coastal wharf structures, and there is still a significant amount of space for processing and studying monitoring data. Based on an anode-ladder sensor monitoring system deployed at a high-piled wharf in Tianjin Port, the long-term durability monitoring of the high-piled wharf is achieved, and also accumulating relevant monitoring experience on high-piled wharf. According to 4-years continuous monitoring, 40

parameters related to the anode rods were collected, including current, voltage, resistance, and ambient temperature. The conclusions drawn from this study is shown as follows:

(1) Correlation analysis of the anode-ladder monitoring data using the Pearson correlation coefficient indicated a strong correlation between the voltage and current values of anode rods A1–A6 relative to the cathode. Additionally, a strong correlation existed between the voltage and current values relative to the reference electrode.

(2) Prediction analyses of the voltage and current values for anode rods A1–A6 using the BP neural network, PSO-BP prediction method, and GABP prediction method showed that the GABP method had the best prediction performance. The R^2 values for the predicted voltage and current values of anode rods A1–A6 are all more than 0.80, indicating high prediction accuracy, and further demonstrating the practicality and generalization ability of the GABP method.

REFERENCES

[1] Z. W. Gan, M. RAUPACH, W. L. Jin, et al, "In-situ monitoring and early warning system for durability of concrete structure of Hangzhou Bay Bridge," China Journal of Highway and Transport, vol. 23, no. 2, pp30-35, 2010.

[2] W. L. Jin, Q. F. Lv, Y. X Zhao, et al, "Research progress on durability design methods and life prediction of concrete structures," Journal of Building Structures, vol. 28, no. 1, pp7-13, 2007.

[3] J. Q. Li, J. B. Xiong, Z. H. Fan, et al, "Research progress and prospect of macro cell corrosion of steel bars in concrete," Journal of the Chinese Ceramic Society, vol. 49, no. 8, pp1631-1641, 2021.

[4] M. Raupach, P. Schiessl, "Monitoring system for the penetration of chlorides, carbonation and the corrosion risk for the reinforcement," Construction and Building Materials, vol. 11, no. 4, pp1631-1641, 1997.

[5] M. Raupach, P. Schieβl, "Macrocell sensor systems for monitoring of the corrosion risk of the reinforcement in concrete structures," NDT&E International, vol. 34, no. 6, pp435-442, 2001.

[6] Q. Chen, X. B. Song, Z, Y. Zhai, "Experimental study on critical chloride ion concentration of reinforcement corrosion in simulated pore fluid of concrete," Sichuan Building Science, vol. 34, no. 6, pp1631-1641, 2008.

[7] C. M. Hansson, A. Pousaee, A. Laurent, "Macrocell and microcell corrosion of steel in ordinary portland cement and high performance concretes," Cement and Concrete Research, vol. 36, no. 11, pp2098-2102, 2006.

[8] X. Wang, Z. J. Chen, G. Xu, "Corrosion monitoring in anchorage area of Sutong Bridge based on anode ladder system," Journal of Building Science and Engineering, vol. 29, no. 4, pp106-111, 2012.

[9] F. M. Li, Y. S. Yuan, O. Geng, "Theoretical model of reinforcement corrosion rate in concrete," Journal of South China University of Technology (Natural Science Edition), vol. 37, no. 8, pp83-88, 2009.

[10] M. J. He, Y. Z. Ye, F. H. Li, "Research on embedded anode ladder monitoring system," Materials Review, vol. 24, no. 24, pp79-82, 2010.

[11] H. B. Liu, Z. F. Ji, S. L. Zhang, et al, "Research on durability monitoring and automatic control technology of new high pile pier based on anode ladder sensor," Journal of Waterway and Harbor, vol. 40, no. 6, pp680-686, 2019.

[12] Z. G. Sun, Y. W. Guo, Y. F. Fan, "Experimental study on concrete durability monitoring with trapezoidal anode system," Structural Engineer, vol. 35, no. 6, pp148-153, 2019.

[13] A. Chauhan, U. K. Sharma, "Influence of temperature and relative humidity variations on non-uniform corrosion of reinforced concrete," Structures, vol. 19, pp296-308, 2019.

[14] X. L. Gu, A. M. ASCE, Z. Dong, et al, "Corrosion of stirrups under different relative humidity conditions in concrete exposed to chloride environment," American Society of Civil Engineers, vol. 32, no. 1, pp1631-1641, 2020.

[15] H. B. Liu, H. C. Liu, F. L Qi, et al, "Study on durability monitoring of high pile wharf based on anode ladder sensor," Journal of Waterway and Harbor, vol. 44, no. 3, pp422-431, 2023.

[16] T Zhang, O. E. Gjørv,"Diffusion behavior of chloride ions in concrete," Cement and Concrete Research, vol. 26, no. 6, pp907-917, 1996.

[17] C. Xu, Z. Y. Li, W, L. Jin, "A new corrosion sensor to determine the start and development of embedded rebar corrosion process at coastal concrete," Sensors, vol. 13, no. 10, pp13258-13275, 2013.

[18] M. J. He, X. R. Li, "Quantitative determination of corrosion status of rebar by electrochemical parameters," Academic Journal of Architecture and Geotechnical Engineering, vol. 3, no. 1, pp32-40, 2021.

[19] ASTM International C 876-09 (2009). "Standard test method for corrosion potential of uncoated reinforcing steel in concrete," Available online: http://www.astm.org/c0876-15.html.

[20] I. Cohen, Y Huang, J Chen, et al, "Pearson correlation coefficient," Noise Reduction in Speech Processing, vol. 2, pp1-4, 2009.

[21] H. Zhang, C. Long, S. Y. Hu, et al, "Topology verification method of distribution network based on hierarchical clustering and Pearson correlation coefficient," Power System Protection and Control, vol. 49, no. 21, pp88-96, 2021.

[22] L. P. Dong, Q. H. Nie, X, K. Sun, et al, "Analysis of influence of shield tunneling parameters on surface settlement based on Pearson correlation coefficient method," Construction Technology, vol. 53, no. 1, pp116-123, 2024.

[23] S. Santosa, R. A. Pramunendar, D. P. Prabowo, and Y. P. Santosa, "Wood types classification using back-propagation neural network based on genetic algorithm with gray level co-occurrence matrix for features extraction," IAENG International Journal of Computer Science, vol. 46, no.2, pp149-155, 2019.

[24] Y. B. Wang, Y. Duan, Y. Y. Li, et al, "Smoke recognition based on dictionary and BP neural network," Engineering Letters, vol. 31, no.2, pp554-561, 2023.

[25] K. Cui, X. Jing, "Research on prediction model of geotechnical parameters based on BP neural network," Neural Computing and Applications, vol. 31, pp8205-8215, 2019.

[26] S. B. Zhang, T. X. Wang, S. J. Wang, et al, "State of charge estimation model for lithium-ion batteries based on deep learning neural networks," Engineering Letters, vol. 32, no.2, pp209-219, 2024.

[27] S. F. Dong, C. Y. Su, J. Z. Yu, "An optimizing BP neural network algorithm based on genetic algorithm," Artificial Intelligence Review, vol. 36, pp153-162, 2011.

[28] Y. Y. Bao, Y. Liu, J. S. Wang, et al, "Genetic algorithm based on grid maps for solving robot path planning problem," Engineering Letters, vol. 31, no.4, pp1635-1648, 2023.

[29] M. H. Zhao, Y. P. Zhao, C. X. Ma, et al, "Robust optimization of mixed-load school bus route based on multi-objective genetic algorithm," Engineering Letters, vol. 30, no.4, pp1543-1550, 2022.

[30] H. Xie, P. Lin, J. T. Kang, et al, "Prediction method of rock uniaxial compressive strength based on feature optimization and SSA-XGBoost," Sustainability, vol. 16, no. 19, pp8460, 2024.

[31] X. J. Li, F. Y. Zhang, F. Yu, "Wind power spare parts demand prediction based on principal component analysis and BP neural network," Science Technology and Engineering, vol. 24, no. 1, pp281-288, 2024.

Hongbiao Liu was born in February 1981 and received his Ph.D. in Structural Engineering from the Institute of Engineering Mechanics, China Earthquake Administration in 2012. He has been a Professor of structural engineering at Tianjin Research Institute for Water Transport Engineering of China since 2022, where he currently studies the structural health monitoring of wharf.

Hongbiao worked in the Tianjin Research Institute for Water Transport Engineering of China from 2012-2024, where he conducted research mainly on visual inspection technology and assessment methods of hydraulic structural engineering, including wharfs and long-span bridges in coastal ports. He has published more than 30 articles in several international journals and is currently paying more attention to research regarding the health monitoring technology of costal wharfs and durability evaluation methods of wharf in costal ports.